Petroleum Science 23 (2026) 1712–1727

Contents lists available at ScienceDirect

Petroleum Science

journal homepage: www.keaipublishing.com/en/journals/petroleum-science

Original Paper

Pore preservation mechanism and conceptual model of fine-grained sedimentary rocks of Qiongzhusi Formation in Deyang–Anyue rift trough, Sichuan Basin

Dan-Dan Wang [a,b], Zhen-Xue Jiang [a,b,*], Ma-Jia Zheng [c], Ya Wu [c], Huan Miao [a,b], Zhi-Kai Liang [d], Yuan-Hao Zhang [a,b], Da-Dong Liu [a,b], Xiang-Lu Tang [a,b]

[a] National Key Laboratory of Petroleum Resources and Engineering, China University of Petroleum (Beijing), Beijing, 102249, China
[b] College of Geosciences, China University of Petroleum (Beijing), Beijing, 102249, China
[c] Development Division of Southwest Oil and Gas Field Branch of China National Petroleum Corporation, Chengdu, 610051, Sichuan, China
[d] School of Geosciences, Yangtze University, Wuhan, 434023, Hubei, China

ARTICLE INFO

Article history:
Received 18 June 2025
Received in revised form
26 August 2025
Accepted 16 December 2025
Available online 19 December 2025

Edited by Xi Zhang and Jie Hao

Keywords:
Sichuan Basin
Qiongzhusi Formation
Pore preservation mechanism
Shale gas
Conceptual model

ABSTRACT

To elucidate the role of effective pore preservation in controlling shale gas enrichment and high yield. This study focuses on fine-grained sedimentary shale of the Qiongzhusi Formation in Sichuan Basin, sampled from different tectonic settings. Rock facies were classified based on total organic carbon (TOC) measurements, X-ray diffraction (XRD), and cast thin section observations. The same lithofacies shale was selected for multi-scale pore characterization and field emission scanning electron microscopy (FE–SEM) to identify pore types and pore structures. By integrating actual drilling and logging data, paleopressure reconstruction via methane inclusion Raman spectroscopy, and burial history analysis of gas reservoirs, the preservation conditions of gas reservoirs are clarified. This study systematically reveals the mechanisms of shale pore preservation at different tectonic settings under the coupled effects of mineral composition, sealing systems, and fluid overpressure. A conceptual model for pore preservation in the Qiongzhusi Formation shales is further proposed. The results show that the deep shelf shales within the rift trough is characterized by high TOC, a rigid mineral skeleton, and overpressure storage. These shales develop an organic–inorganic composite pore network, exhibiting significantly higher pore volume and gas yield compared to shales outside the trough. At the trough margin, a semi-closed system with plastic mineral framework and moderate overpressure supports medium porosity. In contrast, shales outside the rift trough exhibit the weakest pore preservation capacity due to an open system, normal pressure, and plastic mineral framework. This study proposes a ternary synergistic pore preservation model of "rigid skeleton–closed system–hydrocarbon fluid overpressure", which provides critical geological insight for the exploration and development of deep fine-grained sedimentary shale gas.

1. Introduction

Shale gas represents one of the most promising unconventional energy resources today. Its efficient exploration and development is crucial for alleviating energy shortage. In China, shale gas production has exceeded 250 × 10^8 m^3 (Guo et al., 2024). In recent years, the ultra-deep areas around the rift trough and paleo-uplift in the Sichuan Basin, Zizhong–Weiyuan area and Jingyan–Qianwei area have achieved exploration breakthroughs in new strata (Cambrian Qiongzhusi Formation), breaking the situation that the production is mainly contributed by the Silurian system (Yong et al., 2024). Significant variations in gas content and single-well production are observed across different tectonic units. Since shale gas accumulates in effective reservoir space, pore formation and preservation run through the whole process of shale gas accumulation and enrichment (Xiang et al., 2024). These processes are influenced by factors such as depositional and diagenetic

* Corresponding author.
E-mail address: jiangzx@cup.edu.cn (Z.-X. Jiang).
Peer review under the responsibility of China University of Petroleum (Beijing).

https://doi.org/10.1016/j.petsci.2025.12.028

history, hydrocarbon generation and expulsion, differential structural uplift and deformation, and formation pressure (Xiang et al., 2024). Therefore, investigating the pore preservation mechanisms in shale reservoirs is essential for successful shale gas exploration and development. Current research on the micro-preservation mechanisms of shale gas has largely focused on the Wufeng–Longmaxi formations, with a prevailing view that these shales are self-sealing (Guo et al., 2024; Jia et al., 2021). However, the Qiongzhusi Formation has experienced deep burial, high maturity and multiple phases of intense tectonic deformation. As a result, the mechanisms of pore preservation in these shales remain inadequately studied and lack comprehensive systematic analysis.

Under similar conditions of burial depth and thermal evolution, pore preservation efficiency varies significantly across different structural settings. Conventional interpretations often emphasize control by a single factor, such as rigid mineral content or overpressure intensity (Zhu, 2024). For instance, rigid minerals are thought to resist compaction and preserve pores. For example, the 'triangular stress' is formed between pyrite particles in the organic matter and pyrite aggregate combination (Yu et al., 2024), Which helps maintain rounded pores under relatively uniform stress. In contrast, pores associated with clay–organic composites tend to be elongated and more susceptible to compaction due to the plasticity of clay minerals and organic matter. Alternatively, some researchers highlight the role of fluid overpressure in pore preservation, suggesting that overpressure counteracts part of the overburden stress (Li et al., 2020, 2024). The Qiongzhusi Formation exhibits distinctive sedimentary characteristics, with interbedded shales and silty shales forming multiple vertical "compartment systems" (Guo et al., 2024; Liang et al., 2021; Liu, 2023). The structural heterogeneity of these compartments influences source rock hydrocarbon generation and expulsion efficiency, as well as the sustained overpressure support for pores, has often been neglected in previous studies.

While it is widely accepted that structural deformation damages pore systems (Xiang et al., 2024). Different tectonic events introduce varying magnitudes of stress. The architecture of the sealed compartment and the degree of system overpressure control the mineral–pore interfaces in shale reservoirs, leading to differing degrees of pore deformation or collapse (Guo et al., 2021; Wang et al., 2020, 2025; Yu et al., 2024; Zhang et al., 2022). Thus, pore preservation is governed by the interplay among mineral–pore contacts, compartment sealing capacity, and the evolution of the pore pressure system under different tectonic conditions (Liu et al., 2022). To date, the pore preservation mechanism in the Qiongzhusi Formation shales has not been fully revealed, particularly the coupling effects of multiple influencing factors. This study focuses on fine-grained sedimentary shales of the Qiongzhusi Formation from inside and outside the Deyang–Anyue rift trough in Zizhong–Weiyuan area. By investigating shale lithofacies composition, pore structure characteristics, preservation conditions, compartment systems, and pore pressure evolution, we aim to reveal the pore preservation mechanisms in these fine-grained sedimentary rocks and establish a conceptual model for pore preservation.

2. Geological backgrounds

The Sichuan Basin, a typical superimposed petroliferous basin and the primary production area for shale gas in China, is situated in the western part of the Upper Yangtze Plate. It exhibits a rhomboid-shaped geometry with a general east–west trend (Fan et al., 2021; Xiong et al., 2023; Zhao et al., 2019). The study area is located mainly in the southeastern part of the Leshan–Longnvsi Paleo-uplift, characterized by an east–west zonation and north–south block division (Fan et al., 2021; Liu, 2023). Affected by the Tongwan movement at the end of the Dengying Formation deposition, the strata experienced significant uplift and denudation, leading to the formation of the Deyang–Anyue rift trough, which generally trends north–south (Fig. 1(a) and (c)). The study area has undergone multiple phases of tectonic deformation, including the Caledonian, Indosinian, Yanshan, and Himalayan movements, resulting in a structural framework that is deep in the north and shallow in the south, with a steep eastern flank and a gentle western slope. It can be subdivided into three major tectonic units: the highland outside the trough, the slope along the trough margin, and the center of the trough. These units were influenced by sediment sources such as the Kangdian ancient land, western Sichuan, a small amount of Motianling and Hannan ancient land (Xiong et al., 2023). Thick black shale and silty shale were vertically superimposed in the center of the trough during the deposition of the Qiongzhusi Formation (Fig. 1(c)). According to the lithology, electrical and geochemical characteristics, it is divided into Qiong1 and Qiong2 sections. The Qiong1 section is divided into Qiong1^1 member (1st–4th layers) and Qiong1^2 member (5th–6th layers), while the Qiong2 section comprises the 7th and 8th layers. Among these, the 1st, 3rd, 5th and 7th layers are black shale, whereas the 2nd, 4th, 6th and 8th layers are silty shale or silty-fine sandstone. Currently, the key development layer is 5th layer (Fig. 1(b)). The Qiongzhusi Formation shale overlies the Canglangpu Formation limestone. Within the rift trough, it is in conformable contact with the underlying Maidiping Formation, whereas outside and along the margins of the rift trough, it rests unconformably upon the Dengying Formation limestone (Fig. 1(c)).

3. Samples and methods

3.1. Samples

Samples from the Qiongzhusi Formation were collected from the periphery of the Deyang–Anyue rift trough in the Sichuan Basin, with primary data sourced from wells Q1–Q3. The drill site locations are shown in Fig. 1(a), where Q1 well is located in the western highland outside the trough, Q2 well is located on the slope of the trough margin, and Q3 well is located in the center of the trough (Fig. 1(c)). All samples were obtained from 5th layer (Fig. 1(b)). Particle size analysis of fine-grained sedimentary rocks was conducted through core observation, cast thin-section identification, and processing with ImageJ software. Geochemical characteristics and mineral composition of the shales were determined based on TOC measurement, XRD analysis, and laser Raman spectroscopy of organic matter. Reservoir pore characteristics were evaluated using a combination of gas adsorption (CO_2 and N_2), high pressure mercury injection, FE–SEM and digital image analysis. Methane inclusion densities were estimated by measuring the Raman spectral shift of methane within fracture veins, and the capture pressures of these inclusions were calculated using an equation of state for a supercritical methane system. Combined with basin numerical simulation technology, actual drilling, logging data and reservoir physical properties, the differences in preservation conditions such as vertical roof and floor sealing, storage box structure and pore pressure evolution of fine-grained sedimentary shale are identified. And then the pore preservation mechanism of fine-grained sedimentary rocks in Qiongzhusi Formation of Sichuan Basin was revealed and a conceptual model was established.

3.2. Methods

In this study, the casting thin section identification, TOC content determination, XRD experiment and FE-SEM experiment

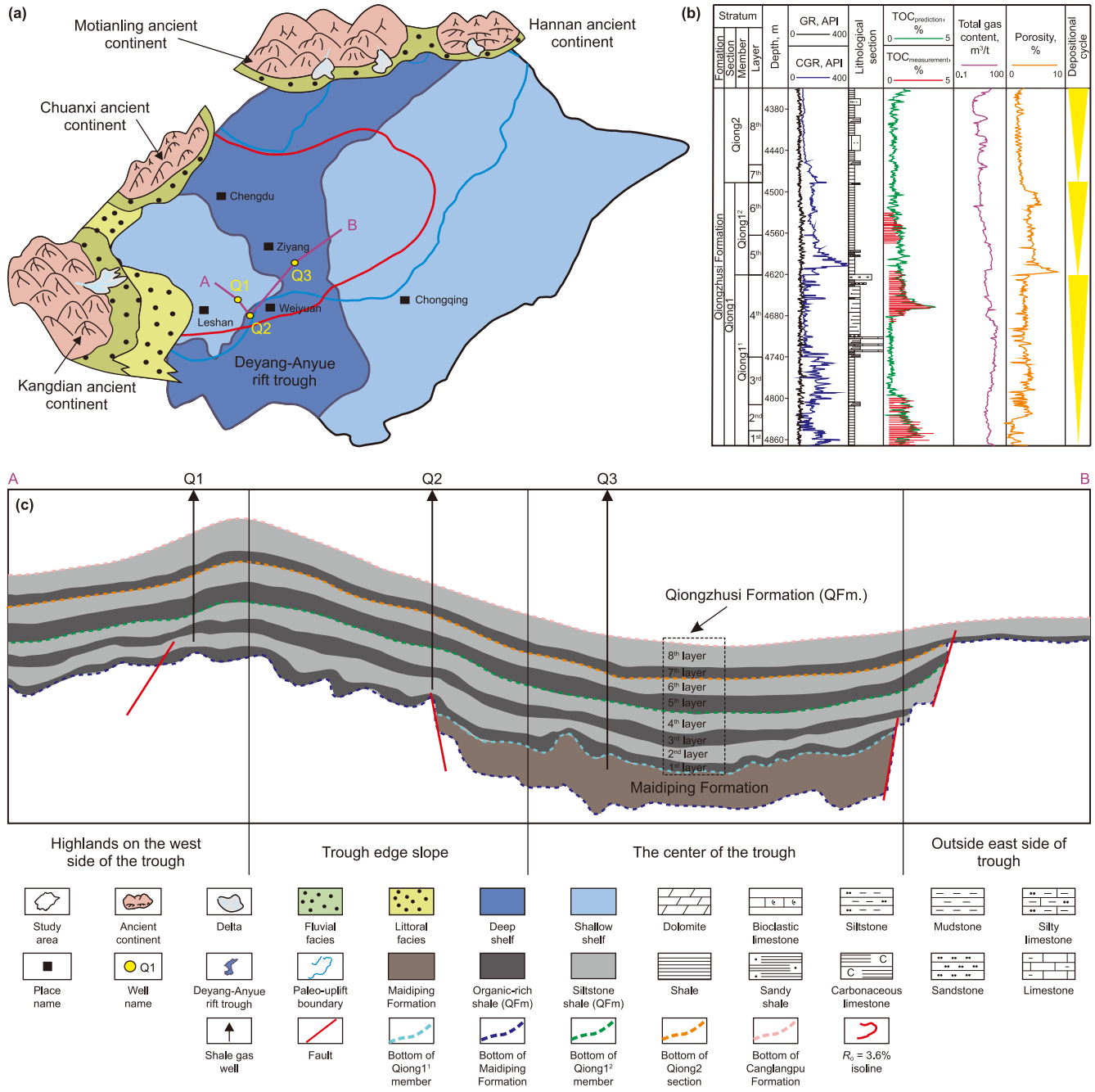

Fig. 1. **(a)** The geographical location of study area. **(b)** The Q3 single well histogram. **(c)** The cross section of Qiongzhusi Formation through Q1–Q3 wells.

were all completed in the Beijing State Key Laboratory of China University of Petroleum. TOC content was measured using CS844 carbon and sulfur analyzer of Lectra company in the United States. Samples were first pretreated with dilute hydrochloric acid (HCl) in a water bath to remove inorganic carbon, then rinsed with deionized water and dried in an oven prior to analysis. All measurements were conducted under standard laboratory conditions (23 °C, 30% humidity, and standard atmospheric pressure). XRD analysis was conducted using X'Pert Powder X-ray diffractometer. Samples were crushed to 200 mesh, dried, and leveled on a glass slide before scanning at a speed of 2 °/min with a step size of 0.02°. Mineral compositions were interpreted using Jade 6.5 software. Argon ion polishing was carried out at Beijing Dongfang Zhisheng Testing Company. The surface of the polished sample was sprayed with carbon, and then the image was observed by Zeiss scanning electron microscope.

Solid bitumen Raman spectroscopy and multi-scale pore size characterization of shale reservoir (including CO_2, N_2 adsorption and high pressure mercury intrusion) were completed in Beijing Craton Testing Company. Both organic matter enrichment and gas adsorption experiments required 80–200 mesh powdered samples. Organic matter enrichment involved treating samples with HCl and HF, rinsing to neutral pH, followed by centrifugation, ultrasonic separation, and drying. The purified kerogen was mixed with epoxy resin in a 3:1 ratio, cured, and polished to a mirror surface. Raman spectra of solid organic matter were acquired

using a Horiba HR800 micro-laser Raman spectrometer. The system was calibrated using a single-crystal silicon wafer peak at 520.7 cm^{-1}. Spectra were accumulated 3 times with an exposure time of 5 s per acquisition.

Gas adsorption analysis was performed on an ASAP 2460 automated surface area and porosity analyzer using 80 mesh powder. The specific surface area measurement range is greater than 0.01 m^2/g, and the pore size range is 0.35–500 nm. The mercury intrusion experiment was completed by using the American AutoPore IV 9500 mercury intrusion instrument, including the process of pressurized mercury injection and decompression mercury withdrawal. The samples need to be processed into blocks or columns. The maximum intrusion pressure exceeded 200 MPa. Total pore volume and specific surface area were calculated using DFT and BET models, respectively. A weighted average method was applied to integrate pore size distributions across the 2 nm and 50 nm ranges. The thin sample polished by argon ion was sprayed with carbon, and then observed by Zeiss scanning electron microscope, and the pores were identified by Image J software. The process included image binarization, noise reduction processing and threshold segmentation. Finally, the pore structure parameters are extracted, including pore diameter, area, perimeter, Feret diameter, etc. The Feret diameter represents the length of the maximum elongation direction of the pore, which can reflect the degree of deformation of the pore by the external stress. The larger the Feret diameter, the greater the stress deformation. The roundness is mainly calculated by Eq. (1), which can reflect the shape of the pore.

$$\text{Roundness} = \frac{4\pi \cdot S}{C^2} \tag{1}$$

where S is the pore area, C is perimeter. Roundness values range from 0 to 1; values closer to 1 indicate higher circularity and lower deformation.

The Raman spectral shift of methane inclusions within fracture veins was analyzed at the China Petroleum Exploration and Development Research Institute. The samples were made into thin slices, and the composition of inclusions was determined by horiba evolution HR Raman spectrometer produced in France. A 473 nm laser was used for the experiment. The collection time was more than 10 s, and the total number of times was 3 times. After the determination of the spectrum, the base signal was deducted and the peak was found.

The basin simulation technology is to use PetroMod software to simulate the burial history and thermal history of the basin. Based on the lithology and stratigraphic stratification data of drilling and logging, combined with the sedimentary denudation rate, sedimentary denudation uplift period, organic geochemical parameters and boundary conditions such as paleo-water depth, paleogeothermal and paleo-geothermal flow values in the study area (He et al., 2011; Li, 2021; Mei et al., 2014; Richardson et al., 2008; Rao et al., 2013; Su, 2021; Shi et al., 2024; Xu et al., 2012), the 1D model of PetroMod software was used to calibrate the simulation results of thermal history and burial history by using the thermal evolution maturity of organic matter. The actual drilling and logging data can provide information such as formation thickness and lithology. The amount of denudation and paleogeothermal parameters refer to the research results of this area and its adjacent areas. The tectonic movements of the Caledonian and Yanshan–Himalayan periods caused the main amount of denudation, mainly 500–1400 m and 2000–4000 m. For organic geochemical input parameters such as TOC, the original TOC was restored using a material balance method for samples with R_o > 3.0%, with a recovery coefficient of 1.7 (Guo et al., 2019). Tissot_in Waples (1992) _TII_Crack hydrocarbon generation kinetic model was used. Boundary conditions, including paleo-terrestrial heat flow and paleo-temperature, were constrained based on regional geological evidence. The Permian Emeishan mantle plume event resulted in a sharp increase in heat flow, with values reaching 84–90 mW/m^2 during that period, declining to present-day values of 62–64 mW/m^2. The geothermal gradient was set at 2.39–2.5 °C/100 m (Qiu et al., 2021; Rao et al., 2022). Paleo-water depth was reconstructed from sedimentary paleoenvironmental indicators. Trace and rare earth element analyses suggest a water depth of approximately 60 m in the rift trough during the depositional period, and about 35–40 m at the trough margin. Other parameters, including rock thermal conductivity, specific heat capacity, and density, were assigned default values from the software. The simulation results were iteratively calibrated against measured organic matter maturity data until a close match was achieved.

4. Result

4.1. Organic geochemical characteristics and lithofacies

4.1.1. Mineral compositions and organic geochemistry

During the burial of fine-grained sediments in geological history, the pore space of reservoirs evolved with the changes of primary detritus and their assemblages during mechanical compaction and chemical diagenesis (Milliken and Curtis, 2016; Zhang and Li, 2018). Therefore, it is necessary to study the material basis of fine-grained sedimentary shale, including mineral composition and organic geochemical characteristics. The degree of thermal evolution in the study area is generally high. The average of R_o in Q1 well is 3.22%, Q2 well is 3.57%, Q3 well is 3.36%. The overall trend is Q2 > Q3 > Q1, which is in the stage of thermal maturity–over maturity (Fig. 2(a)). The TOC in the center of the rift trough is generally higher than 2% (average 2.31%), and gradually decreases to the outside. The average TOC content of Q2 well is 1.77%, and the average TOC of Q1 well is 1.8% (Fig. 2 (b)). The sedimentary period of the Qiongzhusi Formation is greatly affected by the provenance, especially by the Kangdian ancient land. It is less affected by the western Sichuan, Motianling and the Hannan ancient land, and the filling rate in the rift trough is fast, resulting in a large difference in the mineral composition inside and outside the trough (Fig. 1(a)). The average content of quartz minerals in the 5th layer of Q3 well is 35.3%, feldspar is 31.1%, clay minerals is 32.5%, and carbonate rocks is only 2.1%. The average content of quartz mineral, feldspar, clay mineral and carbonate rock in the 5th layer of Q2 well is 34.5%, 24.2%, 34.7% and 4%, respectively. The average content of Q1 well is 36.5%, 28.0%, 22.1% and 8.14%, respectively (Fig. 2(c)–(f)). It is found that the hydrodynamic force is strong due to the shallow water environment outside the trough, and it is close to the provenance. Fine-grained clay minerals are not easy to deposit, and coarse-grained felsic minerals are more easily enriched. The water is disturbed greatly, the content of carbonate rock is relatively high. The inside rift trough is deep water and the deposition rate is relatively suitable, and fine-grained clay minerals are more easily enriched.

4.1.2. Fine-grained sedimentary particle size and shale lithofacies

From the inside to the outside of the rift trough, the core color gradually becomes lighter (Fig. 3), the particle size distribution can be counted by casting thin section observation and image particle size identification. The shale reservoir in the rift trough has the highest proportion of clay particle content (<3.9 μm) (Fig. 3(a)–(d)) and decreases from the inside to the outside of the trough (Fig. 3(e)–(l)), which is more significantly affected by the

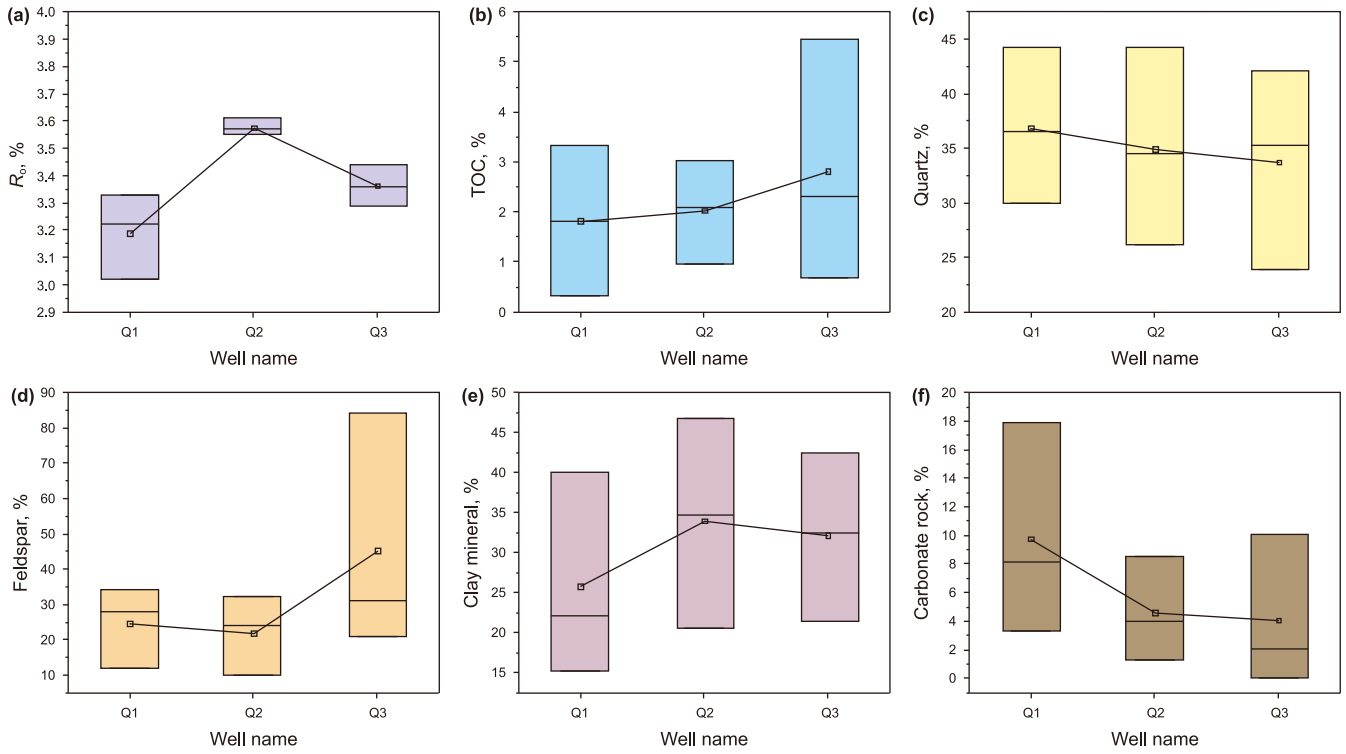

Fig. 2. Mineral composition parameters of organic geochemists in different typical wells inside and outside the rift trough of Qiongzhusi Formation in Sichuan Basin. (**a**) R_o. (**b**) TOC. (**c**) Quartz. (**d**) Feldspar, (**e**) Clay mineral. (**f**) Carbonate rock.

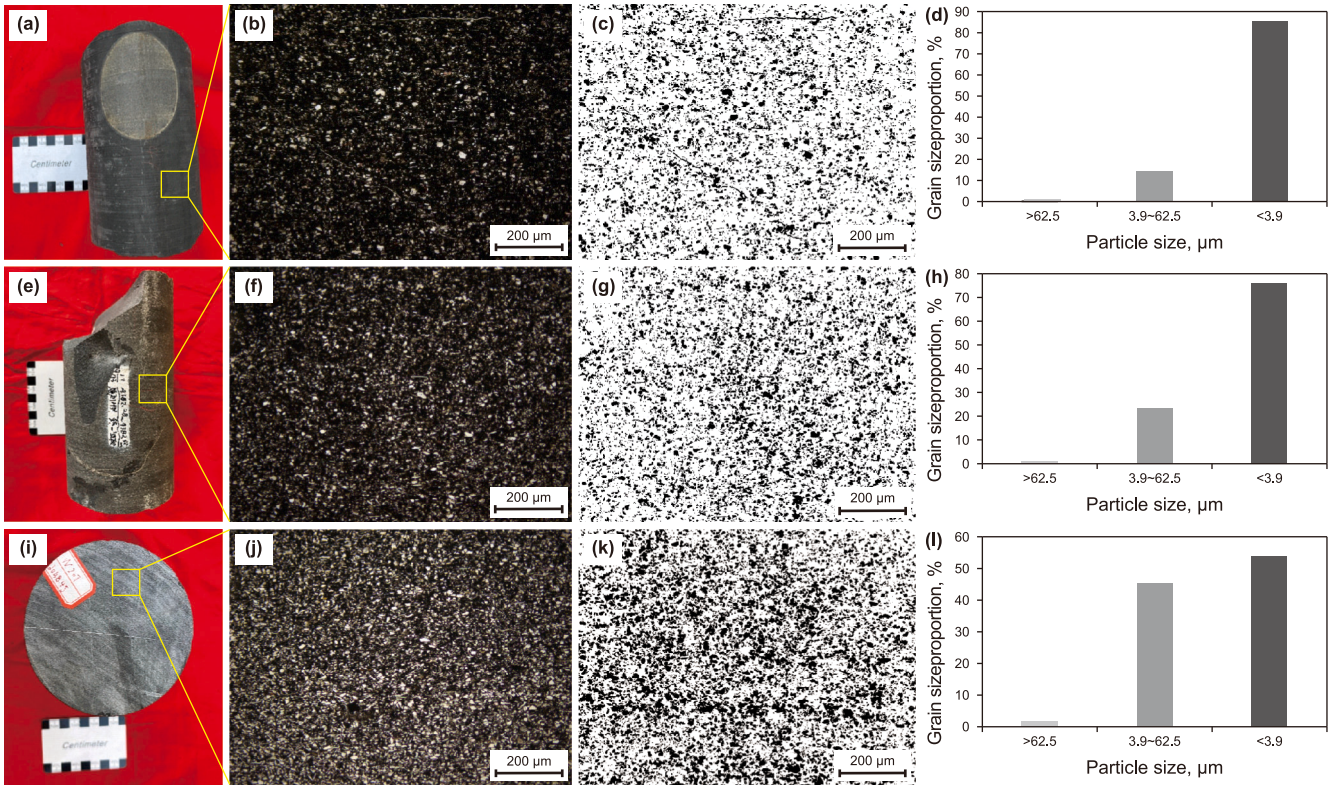

Fig. 3. Core photos, casting thin sections, image grain size identification and grain size distribution proportion characteristics inside and outside the rift trough of Qiongzhusi Formation 5th layer. (**a**)–(**d**) Well Q3, 4560.86 m. (**e**)–(**h**) Well Q2, 4307.5 m. (**i**)–(**l**) Well Q1, 3151.03 m.

hydrodynamic force. This study is mainly based on the definition of fine-grained sedimentary rocks (Aplin and Macquaker, 2011; Milliken, 2014; Lazar et al., 2015), as well as the grain size of fine-grained sedimentary shale, the content of unique/key mineral components, organic matter content for lithofacies division. TOC <1% is defined as organic-poor, 1% < TOC < 2% is defined as organic-contain, and TOC >2% is defined as organic-rich. The felsic mineral content >50% is defined as felsic, the carbonate mineral content > 50% is defined as calcareous, the clay mineral content >50% is defined as clay, and the three mineral content is less than 50% defined as mixed. Sandstone is defined as sand particle content (>62.5 μm) >50%, silty shale is defined as silt particle content (3.9–62.5 μm) >50%, and shale is defined as clay particle content (<3.9 μm) >50% (Guo et al., 2023b) (Fig. 4(a)). The study area mainly develops organic-poor and organic-rich felsic shale facies (Fig. 4(b)–(d)). The water depth in the trough is the deepest, mainly composed of organic-rich felsic shale facies and a small amount of organic-poor felsic silty shale facies (Fig. 4(b)). The water body at the edge of the trough is the most turbulent, and the lithofacies composition is complex, mainly composed of organic-poor felsic shale facies and organic-poor mixed shale facies (Fig. 4(c)). The water outside the trough is the shallowest and the rock particles are the thickest, mainly composed of organic-poor felsic silty shale facies and organic-poor felsic shale facies (Fig. 4(d)).

4.2. Pore development characteristics of fine-grained sedimentary shale reservoir

4.2.1. Pore type of reservoir space

The samples of three wells selected in this study are all organic-contain felsic shale facies. Through field emission scanning electron microscopy observation, it can be seen that there are great differences in pore development in different structural positions of Qiongzhusi Formation shale reservoirs. Inorganic pores are mainly developed, such as mineral intergranular pores between rigid mineral particles (Fig. 5(b), (c), (d) and (f)), dissolution pores (Fig. 5(a), (d) and (f)) are in feldspar and carbonate mineral particles, intercrystal pores (Fig. 5(d) and (g)) are in pyrite, interlayer pores (Fig. 5(h) and (i)) are in clay minerals and multiple rock fractures (Fig. 5(e)) in feldspar. At the same time, a small amount of organic matter pores also developed, which are often associated with pyrite and clay minerals (Fig. 5(g) and (i)). The organic and inorganic pores are well developed inside the trough (Fig. 5(g)–(i)). The organic matter is mainly associated with pyrite, and the shape is round and oval (Fig. 5(g)). There are also some organic pores associated with clay minerals, mostly in a long strip (Fig. 5(i)). The inorganic pores are mainly feldspar dissolution pores and clay mineral intergranular pores (Fig. 5(h) and (i)). The pores developed between organic matter and brittle minerals are long strips. Due to the extrusion of organic matter by hard inorganic minerals, the irregular elliptical organic pores at the edge of organic matter are extruded into long strips (Fig. 5(i)). The organic matter pores in the margin of the trough are relatively less developed, mainly intergranular pores, intragranular and intergranular dissolution pores and rock fracture, and the pore morphology is mostly wedge-shaped (Fig. 5(d)–(f)). The organic pores outside the trough are basically not developed, mainly intergranular pores and dissolution pores, and the pores are irregular in shape (Fig. 5(a)–(c)). The Feret diameter and roundness of fine-grained sedimentary rocks in different structural positions of Qiongzhusi Formation are calculated by Eq. (1) (Fig. 6). The average Feret diameter of Q1 well outside the rift trough is the largest (13.2 nm) (Fig. 6(a)), and the roundness is the smallest (0.488) (Fig. 6). The average Feret diameter of Q3 well inside the rift trough is the smallest (7.6 nm) (Fig. 6(a)), and the roundness is the largest (0.521) (Fig. 6(b)). The Feret diameter of the pores inside and outside the rift trough gradually becomes larger and the roundness gradually becomes smaller. It shows that the pores outside the rift trough are more deformed by external stress, and the pores are flattened and elongated.

4.2.2. Characteristics of reservoir pore structure

Low-temperature N_2 adsorption experiments revealed that the hysteresis loops of the adsorption-desorption curve were H_2 and H_4 types, and the pores were mostly parallel plates or slits (Fig. 7(a)), which was consistent with the results observed under scanning electron microscopy. Combined with CO_2 adsorption and high pressure mercury injection experiments, the full pore size characterization of Qiongzhusi Formation shale inside and outside the rift trough was realized. The results show that the pore volume and specific surface area of the shale in the Qiongzhusi Formation are multimodally distributed (Fig. 7(b) and (c)). The mesopores contribute the most pore volume of the Qiongzhusi Formation, and the total pore volume of macropores and mesopores accounts for more than 90%. A small amount of micropores developed (Fig. 7(b) and (d)), and the contribution of macropores to the total pore

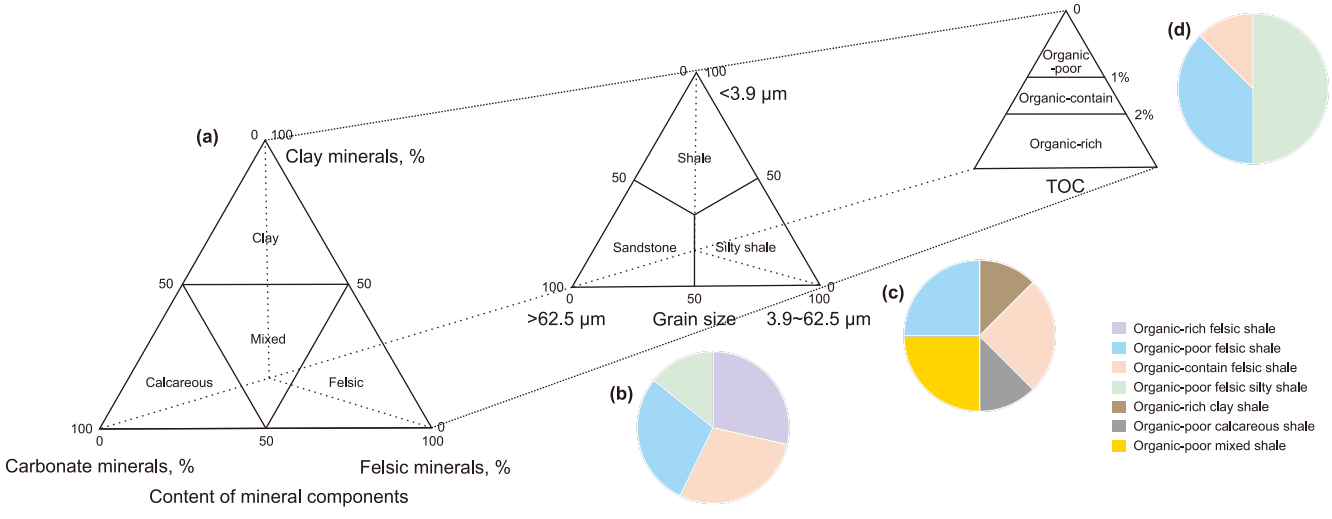

Fig. 4. Lithofacies division diagram and lithofacies classification pie chart of Qiongzhusi Formation inside and outside the rift trough. (**a**) Lithofacies division diagram. (**b**) Pie chart of lithofacies distribution inside rift trough. (**c**) Pie chart of lithofacies distribution at the rift trough margin. (**d**) Pie chart of lithofacies distribution outside rift trough.

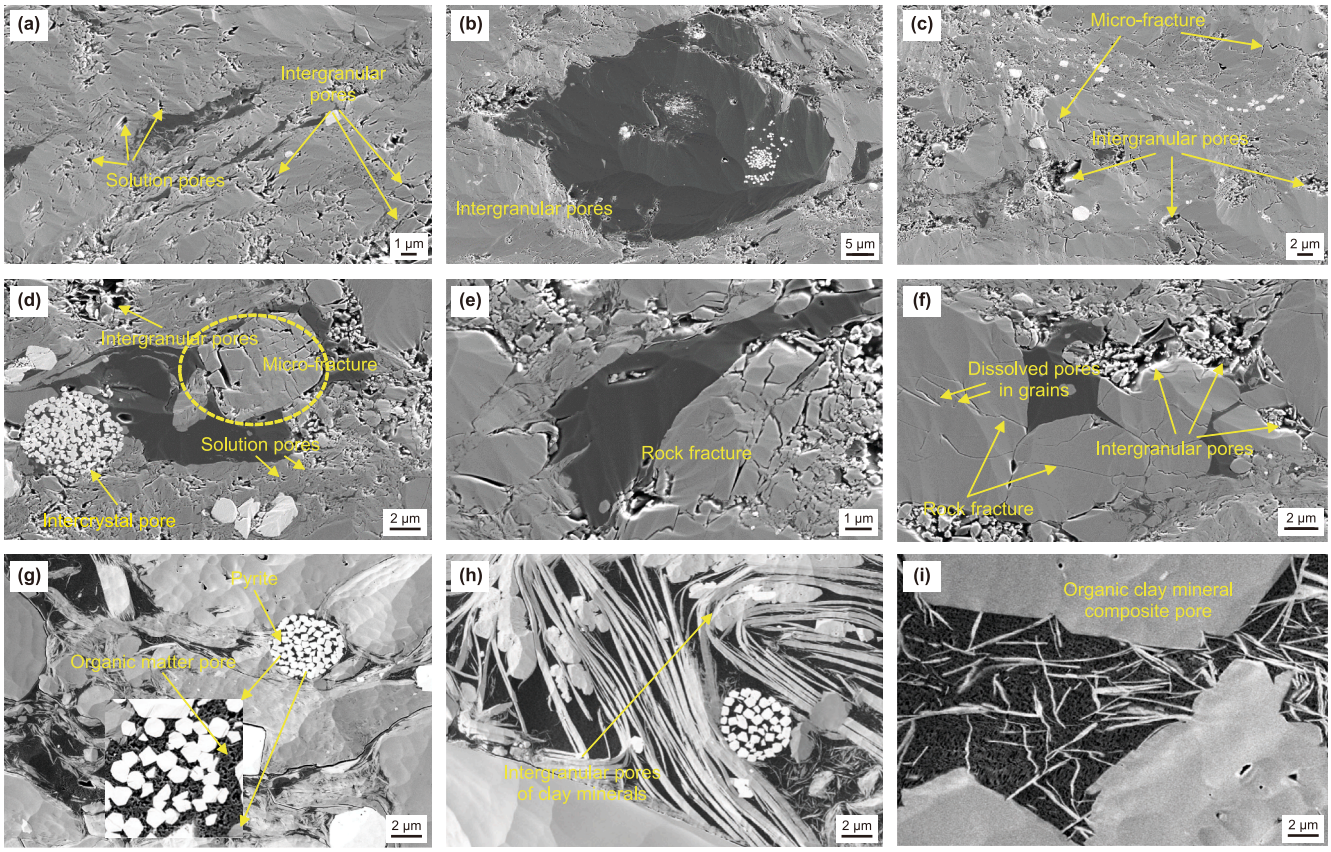

Fig. 5. Scanning electron microscope image of Qiongzhusi Formation in Sichuan Basin. (**a**) The dissolution pores of Q1 well. (**b**) Intergranular pores in Q1 well, organic matter pores are not developed. (**c**) The intergranular pore of Q1 well. (**d**) Intergranular pores, intercrystal pores and dissolution pores in Q2 well. (**e**) Rock fracture of Q2 well. (**f**) Rock fracture and intergranular pore of Q2 well. (**g**) Composite pores of pyrite and organic matter in Q3 well. (**h**) Interlayer pores of clay minerals in Q3 well. (**i**) Composite pores of organic matter and clay minerals in Q3 well.

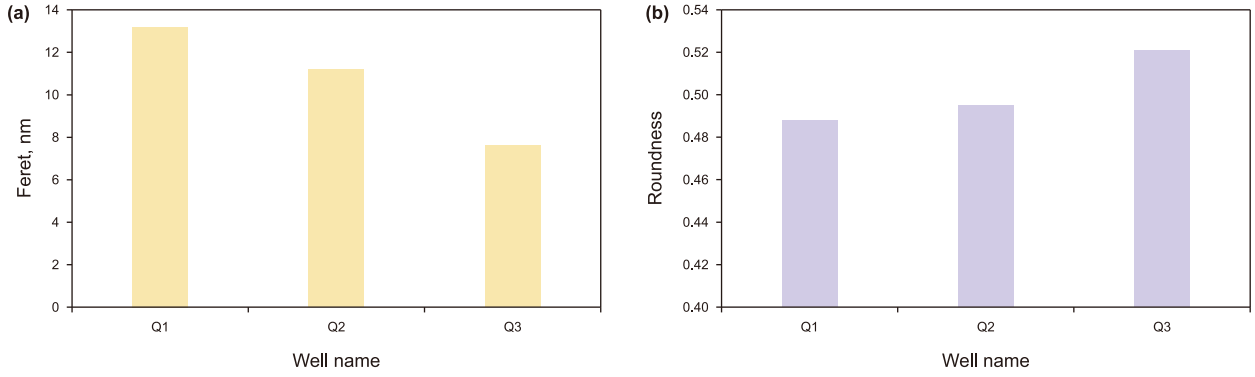

Fig. 6. Shale pore Feret diameter and roundness distribution histogram of typical wells in Qiongzhusi Formation. (**a**) Feret diameter distribution histogram. (**b**) Pore roundness distribution histogram.

volume tends to decrease from the inside to outside of the trough (Fig. 7(d)). The specific surface area is mainly contributed by mesopores and micropores, accounting for more than 99%, and the proportion of mesopores is about 57%–63% (Fig. 7(e)).

4.3. Preservation condition

4.3.1. Sealing property of fine-grained sedimentary shale reservoir system

The sealing system of shale reservoirs refers to a state in which the exchange between the internal fluid (oil and gas, water, etc.) of shale reservoirs and the external environment is significantly limited during the geological history period. This sealing has an important impact on pore preservation. It mainly includes geological sedimentary-structural sealing (cap rock effectiveness), rock physical sealing (reservoir physical parameter difference) and pressure sealing (hydrocarbon fluid overpressure and pressure storage box). Through systematic analysis of the vertical physical property differences, roof and floor characteristics and pressure coefficients of the three wells, it is found that the longitudinal porosity of the Qiongzhusi Formation increases first and then decreases, the porosity of the 3rd–7th layer is larger, the porosity of 5th layer is the largest, and the porosity decreases from the inside to outside of the trough (Q3 > Q2 > Q1). The porosity of the

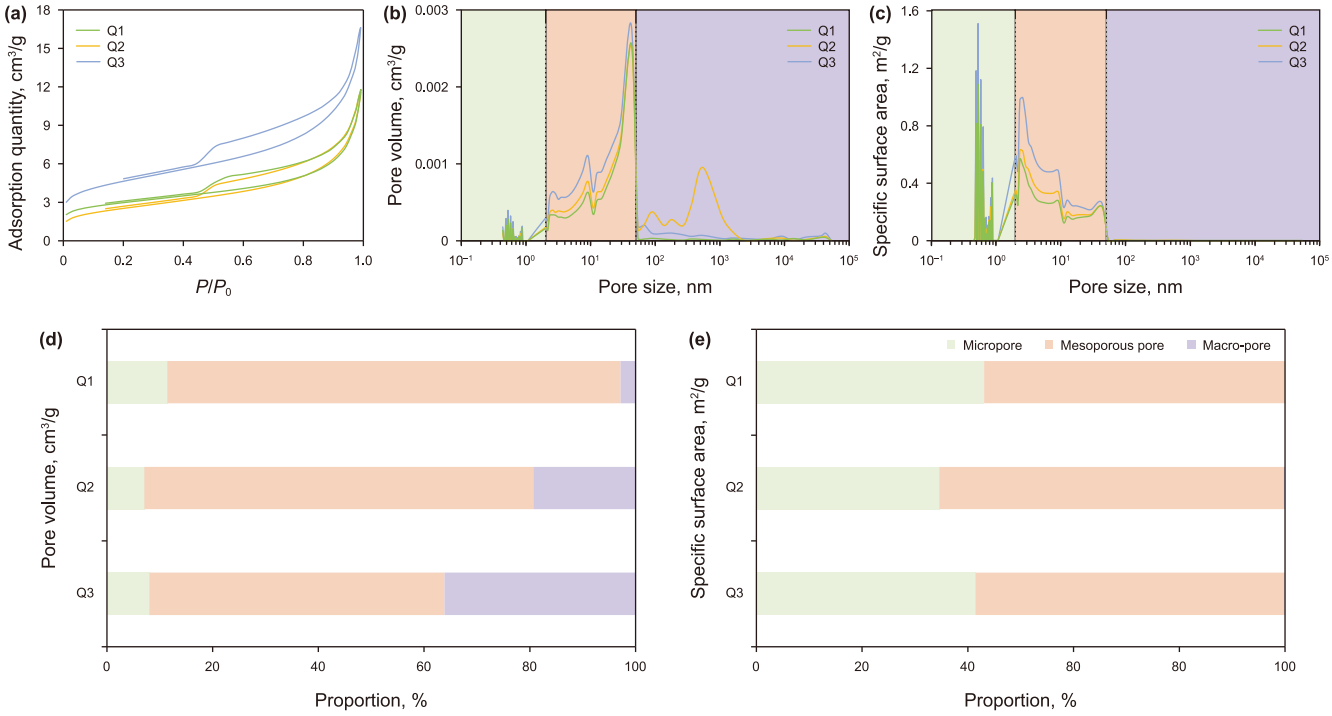

Fig. 7. Pore structure characteristics of fine-grained sedimentary shale in Qiongzhusi Formation, Sichuan Basin. **(a)** Low temperature nitrogen adsorption-desorption curve. **(b)** Pore volume distribution curve. **(c)** Pore specific surface area distribution curve. **(d)** Proportion of pore volume contribution. **(e)** Proportion of pore specific surface area contribution.

two adjacent silty shale layers (4th and 6th layers) are low (Fig. 8(a)). The physical properties of 1st, 2nd and 8th layers are sealed the 3rd–7th layers, and the 4th and 6th layers are sealed the 5th layer in the longitudinal direction (Fig. 8(a)). The development degree of roof is different, and the roof and floor are the overlying and underlying strata directly contacted by the gas-rich strata. The most complete roof (Canglangpu Formation) and floor (Maidiping Formation) are in the rift trough, the thickness is more than 200 m. The edge of the rift trough has a complete roof and a small amount of floor development, only 10 m. Outside the rift trough, the roof is more developed, with a thickness >100 m, but the floor is missing (Fig. 8(b)). The measured pressure coefficient increases gradually from the outside (close to 1) to the inside (close to 2) of the trough, reflecting that the shale reservoir system inside the trough has good preservation conditions, and it is still overpressure today. The preservation conditions of the shale reservoir system outside the trough are poor, and it is normal pressure today (Fig. 8(c)).

4.3.2. Pore pressure evolution

The differential evolution process of different tectonic positions leads to the spatial differentiation of pressure system inside and outside the rift trough of Qiongzhusi Formation shale gas reservoir. The density of methane inclusions is calculated by Raman displacement measurement of methane inclusions (Gao et al., 2014; Li et al., 2018; Wang et al., 2023). Based on the homogenization temperature of gas-liquid two-phase inclusions and the density of methane inclusions in the same period of methane inclusions, combined with the supercritical methane state equation constructed by predecessors, the capture paleopressure of methane gas in inclusions is calculated. The detailed calculation steps can be referred to (Duan et al., 1992; Gao et al., 2014; Li et al., 2018; Wang et al., 2023). The results show that the Raman spectral shift of methane in the Qiongzhusi Formation is between 2909.55 and 2912.2 cm^{-1} (Fig. 9(a)–(d)). The trapping pressure of inclusions outside the trough is 57.0–62.8 MPa (Fig. 9(e)), and the paleopressure coefficient is 1.22–1.31 (normal pressure) (Fig. 10(a)). The trapping pressure of inclusions inside the trough is 109.0–114.20 MPa, and the paleopressure coefficient is 2.13–2.20 (overpressure) (Fig. 9(e)). The burial history and thermal evolution history of the Qiongzhusi Formation were reconstructed by basin simulation technology. It was revealed that the hydrocarbon generation of the thermal evolution of organic matter in the Qiongzhusi Formation in the early–late Cretaceous was continuously enhanced, and the overpressure was gradually accumulated. The initial pressure coefficient can reach more than 2.5 (Fig. 10). In the late Cretaceous tectonic uplift stage, the uplift amplitude in the trough is relatively small (about 1800m), the roof and floor remain intact, and the hydrocarbon generation pressurization rate and the micro-fracture hydrocarbon expulsion rate form a dynamic balance, resulting in the overpressure system continues to be preserved (Q3 well simulation pressure coefficient 2.02), and the porosity decreases proportionally with the burial depth (Fig. 10(c)). The amplitude and rate of the uplift period of the shale gas reservoir at the rift trough margin are also relatively low (about 2500 m). The hydrocarbon generation efficiency is higher than the hydrocarbon expulsion efficiency. The gas reservoir is still overpressure (Q2 well simulation pressure coefficient 1.57), and the porosity also decreases proportionally with the burial depth (Fig. 10(b)). The shale gas reservoir outside the rift trough lacks the floor, and after experiencing the maximum burial depth, the gas reservoir rises by a large amplitude (>2800 m), the hydrocarbon generation efficiency < the hydrocarbon expulsion efficiency, and the overpressure system is destroyed, forming the current normal

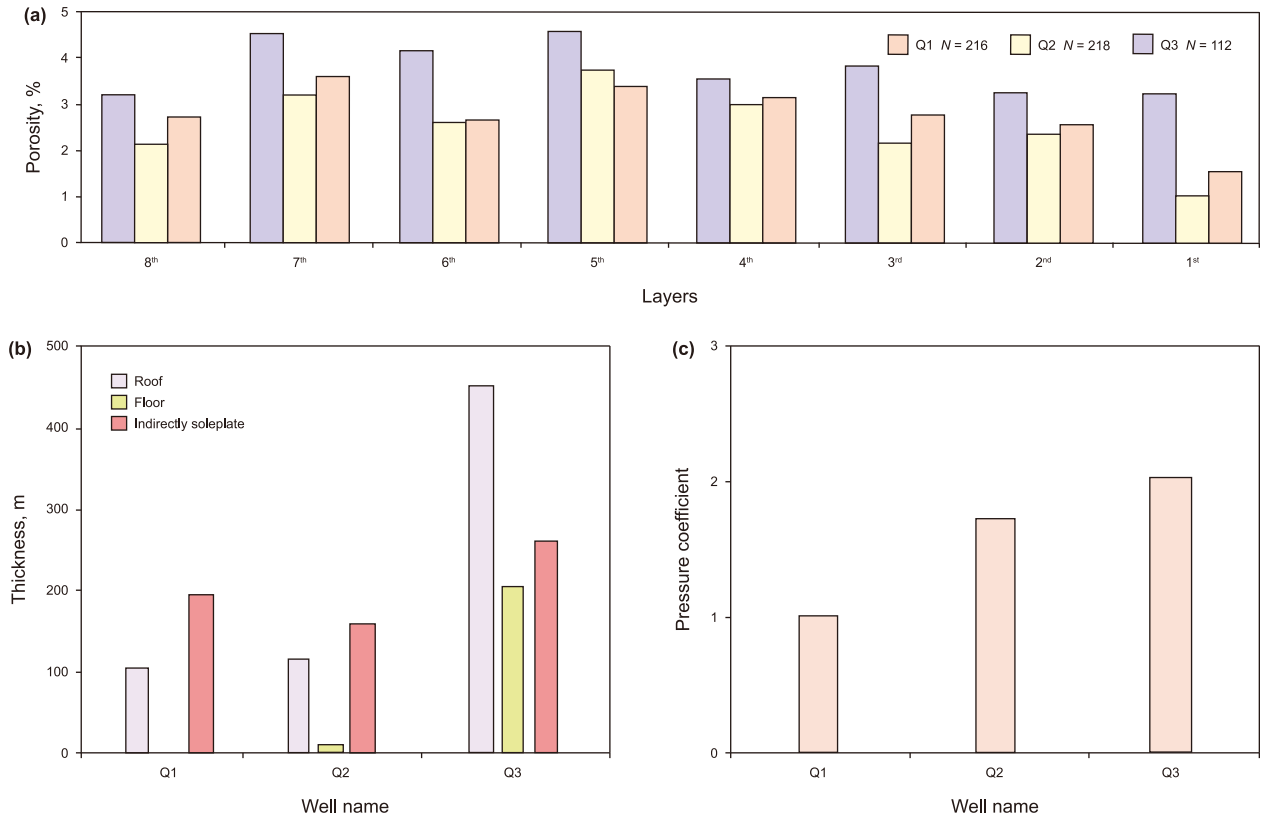

Fig. 8. Shale reservoir preservation conditions of Qiongzhusi Formation in different structural positions of Sichuan Basin. **(a)** Longitudinal porosity distribution histogram. **(b)** The thickness histogram of roof and floor. **(c)** Pressure coefficient distribution histogram.

pressure system (Q1 well simulation pressure coefficient 1.18), and the porosity is greatly reduced with the burial depth (Fig. 10(a)).

5. Discussion

5.1. Pore preservation mechanism of fine-grained sedimentary rock

5.1.1. Effect of mineral composition on pore preservation

Although the mineral composition in shale is complex, it can be divided into rigid pore skeleton and elastic pore skeleton according to the difference of mechanical properties. Quartz is one of the most abundant brittle minerals in shale, which can be generally divided into terrigenous clastic quartz and authigenic quartz. The intergranular pores produced by the early cementation-recrystallization of biogenic siliceous minerals and the late anti-compaction of the quartz lattice generated by them, the former provides effective reservoir space for early asphalt retention, and the latter provides important support and preservation for the primary pores and secondary pores of organic matter (Guan et al., 2021; Nie et al., 2025; Zhao et al., 2019). The sedimentary period of Qiongzhusi Formation in Zizhong–Weiyuan area is close to the provenance (Fig. 1(a)). Clay minerals are usually transported to the deep water area in the high-energy environment (Fig. 2(e)). The environment is mainly dominated by anoxic in the rift trough, with strong adsorption of clay minerals. Organic matter and clay minerals are enriched synchronously to form organic-clay complex, which protects organic matter from biodegradation. Quartz in Qiongzhusi Formation is different from Longmaxi Formation. Quartz in Qiongzhusi Formation has more terrigenous quartz besides authigenic quartz. Rigid mineral framework formed by authigenic quartz combined with other pore-forming minerals can effectively preserve pores. There is a certain correlation between porosity and organic matter content. From the inside to the outside of the trough, the correlation gradually decreases. The porosity in the rift trough is jointly contributed by organic matter pores and inorganic pores. The porosity outside the trough is mainly contributed by inorganic pores. The organic matter pores are relatively undeveloped, which is consistent with the results of scanning electron microscopy and full-aperture characterization (Fig. 5(d), (b) and (h), Fig. 11(a)).

Porosity has a certain correlation with clay minerals and feldspar minerals. Clay and easily dissolved feldspar minerals contribute more to inorganic pores. However, this correlation is gradually weakened from the inside to the outside of the trough, and the porosity of the edge and the outside of the trough is negatively correlated with the clay minerals (Fig. 11(c) and (d)). The porosity in the rift trough is weakly positively correlated with quartz, and the correlation between the edge and the outside of the trough is not obvious (Fig. 11(d)). The authigenic quartz and terrigenous quartz are both developed in the rift trough. The authigenic quartz provides support and preservation for organic matter pores, and together with pyrite, it serves as the rigid framework of the reservoir to avoid feldspar dissolution pores and clay mineral intergranular pores from being compacted by the overlying strata. The effect of quartz as a single mineral on porosity is general. However, the combination of quartz and pore-forming minerals has a positive effect on pore preservation. The correlation between porosity and (quartz + feldspar) and the correlation between porosity and (quartz + clay) are improved compared with the correlation of single minerals, which enhances the contribution of feldspar and clay minerals to pores (Fig. 11(e) and (f)). The water depth at the edge and outside the trough becomes shallow,

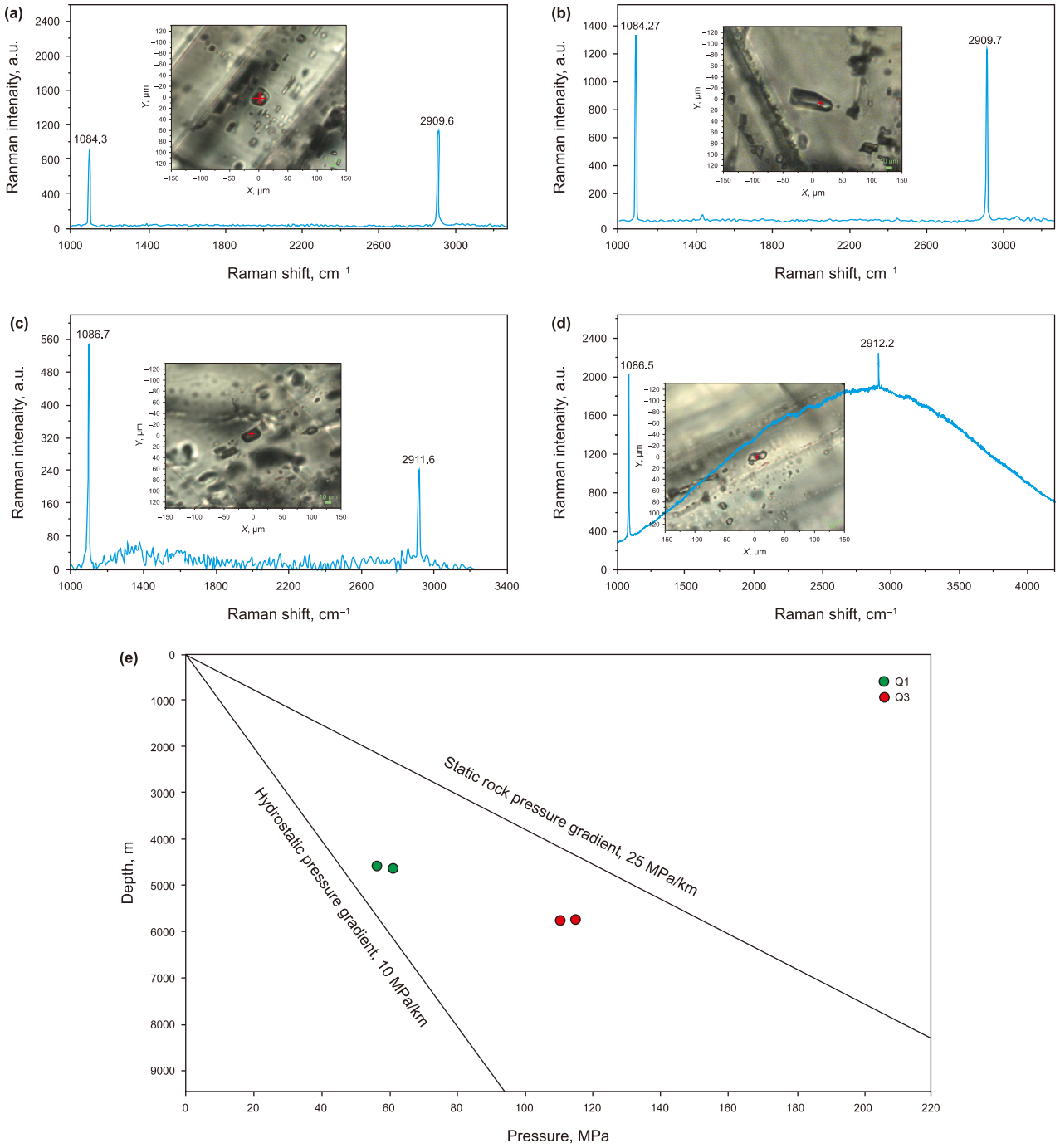

Fig. 9. Raman spectra and pressure distribution of methane inclusions in different structural positions of Qiongzhusi Formation. **(a)–(b)** Raman spectra of methane inclusions in rift trough. **(c)–(d)** Raman spectra of methane inclusions outside the rift trough. **(e)** Pressure distribution characteristics of methane inclusions inside and outside the rift trough.

and the environment transitions to a weak oxidizing environment. The quartz in the reservoir is mostly terrestrial debris, which contributes less to the pore space, and the pyrite is relatively undeveloped. There is no rigid framework in the reservoir, and plastic minerals such as clay minerals are easily compacted by the overlying strata. The higher the clay mineral content, the lower the porosity (Fig. 11(d)). The brittleness of feldspar minerals is relatively large, and the pores are elongated due to the influence of overlying stress (Fig. 5(a) and (b)). Therefore, the combination of rigid minerals and pore-forming minerals outside the trough has no obvious effect on the increase of porosity.

5.1.2. Effect of pressure storage box on pore preservation

The amount of hydrocarbon generation determined by the degree of thermal evolution of organic matter and the amount of hydrocarbon expulsion determined by the closure of the system jointly affect the change of pore pressure. The state of pore pressure and external stress controls the preservation of pores. Too high maturity will cause carbonization of organic matter and rearrangement of macromolecular structure and lead to poor pore development characteristics (Liang et al., 2024; Wang et al., 2014). This can better explain that the development characteristics of organic matter pores in the Qiongzhusi Formation are worse than

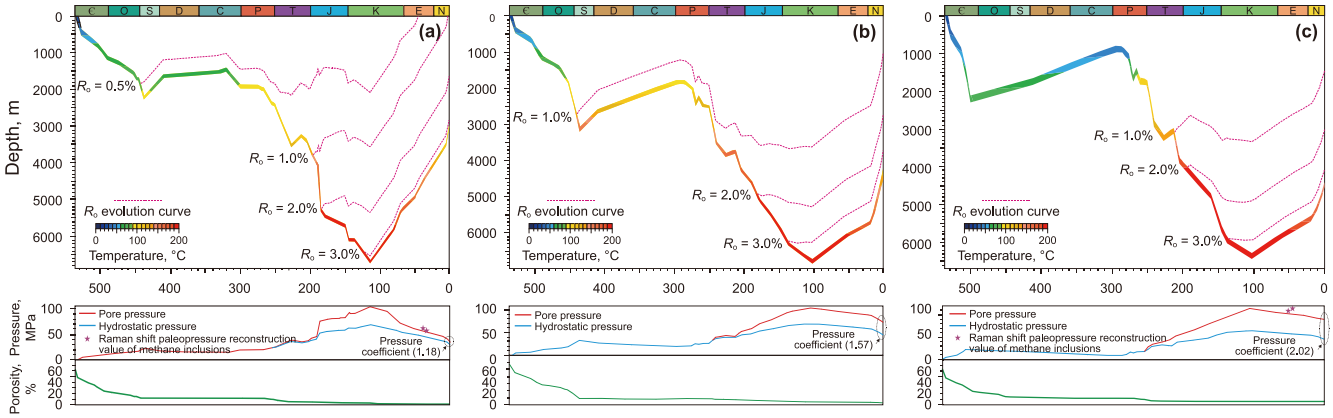

Fig. 10. Burial history and pressure evolution history of Qiongzhusi Formation inside and outside the rift trough. **(a)** Q1 well outside the rift trough. **(b)** Q2 well at the edge of rift trough. **(c)** Q3 well in rift trough.

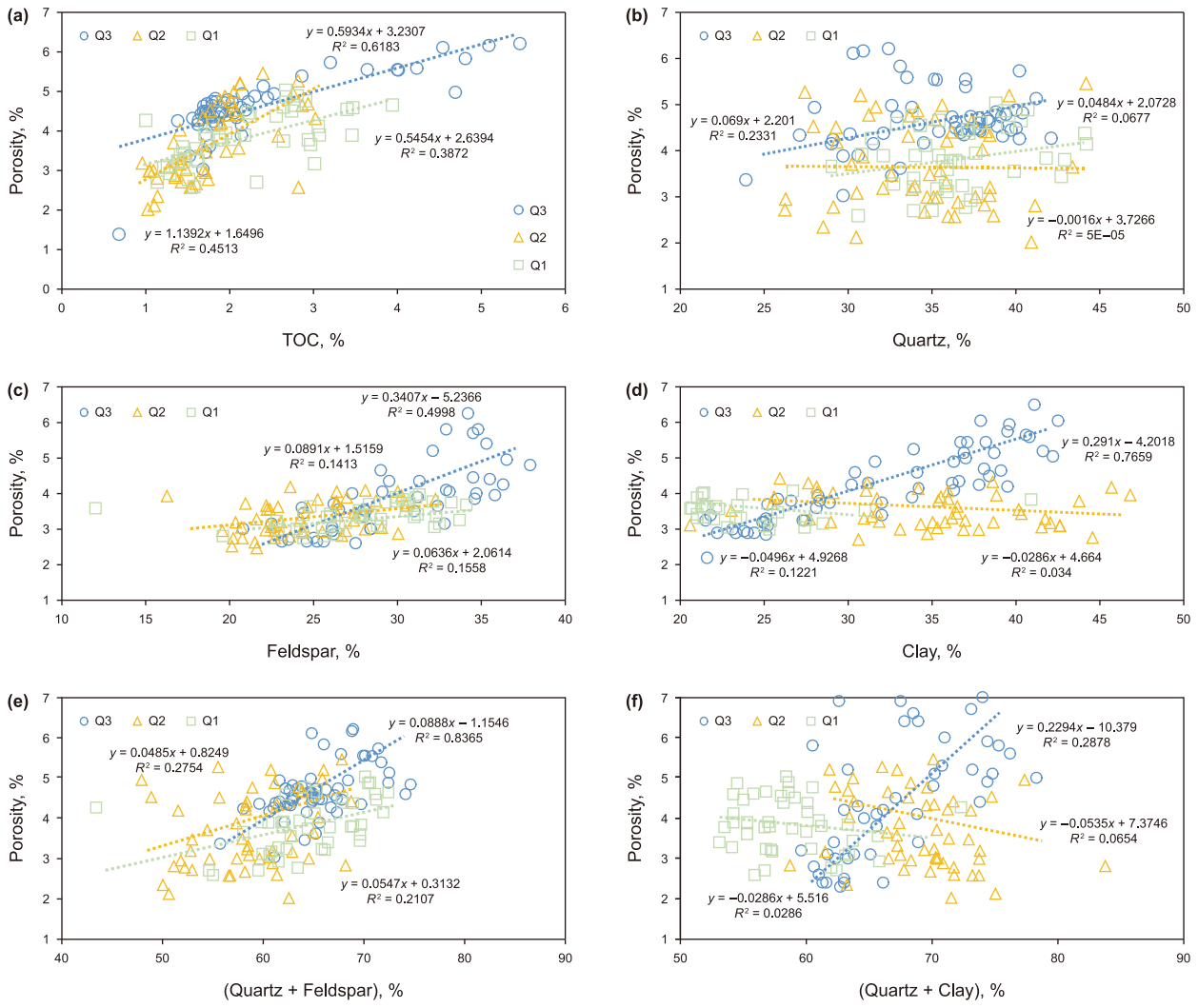

Fig. 11. Correlation between organic matter content, porosity and each component of Qiongzhusi Formation shale. **(a)** Correlation between porosity and TOC. **(b)** Correlation between porosity and quartz. **(c)** Correlation between porosity and feldspar mineral content. **(d)** Correlation between porosity and clay mineral content. **(e)** Correlation between porosity and (quartz + feldspar) mineral content. **(f)** Correlation between porosity and (quartz + clay) mineral content.

those in the Longmaxi Formation with low maturity, but it cannot explain that the Qiong2 section and the Qiong1 section in the study area have similar organic matter types, TOC and have undergone consistent burial and thermal evolution processes, but there are great differences in porosity and organic matter pore characteristics. In fact, the biggest difference between them is the system closure. There are four sets of organic-rich intervals and four sets of corresponding roof and floor sealing layers are

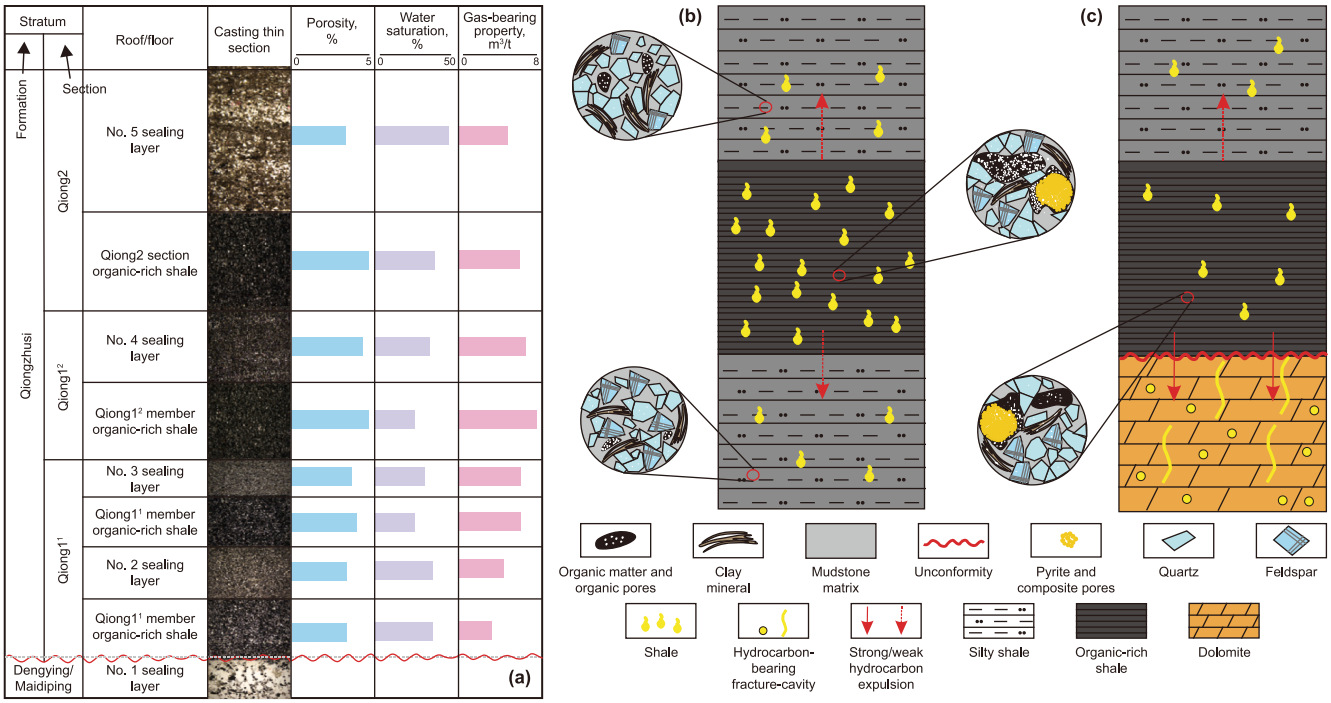

Fig. 12. Vertical storage box structure and compartment system characteristics of Qiongzhusi Formation. **(a)** Vertical storage box distribution. **(b)** Semi-closed-semi-open system. **(c)** Open system.

developed, and there are four storage box structures inside (Fig. 12(a)). The No.1 sealing layer is the floor of the bottom of Qiong1[1] member. Affected by the Tongwan movement, the inside and outside floor of the trough are in integrated and unconformity contact with the Qiongzhusi Formation. The No.2, No.3, No.4 and No.5 sealing layers are all developed in the Qiongzhusi Formation and are in integrated contact with the organic-rich layer. The No.1 sealing layer is weaker than the No.2, No.3, No.4 and No.5 sealing layers in terms of capillary sealing and oil and gas molecular adsorption. There are two types of compartment systems in the vertical direction. One is a semi-closed-semi-open system, which is composed of the top of Qiong1[1] member, Qiong1[2] member, Qiong2 section organic-rich shale layers and their corresponding Nos. 2, 3, 4 and 5 sealing layers as the roof and floor (Fig. 12(a) and (b)). The other is an open system composed of the bottom of Qiong1[1] member, Nos. 1, 2 sealing layers as the floor and roof (Fig. 12(a) and (c)). There are four storage box structures developed inside the trough belong to the semi-closed-semi-open system, and the four storage box structures developed outside the trough include three semi-closed-semi-open systems and one open system. The open system has the characteristics of strong compaction, high water saturation, low porosity, retained hydrocarbon degree, gas content and formation pressure coefficient. The sealing ability of longitudinal capillary is significantly different. The Qiong1[1] member (especially the 1st, 2nd layers) is in an open system outside the trough (Fig. 12(a) and (c)), which are typical 'congenital deficiencies'. Due to the contact of the unconformity surface between the Qiongzhusi Formation and the underlying strata, the hydrocarbon generation and expulsion process is always in an open state, and there is little in-situ retention of hydrocarbons. Therefore, the bottom of Qiong1[1] member with the highest organic matter content has a large amount of hydrocarbon expulsion, low residual hydrocarbon and low pore development due to the unclosed system in the hydrocarbon generation period. It is greatly affected by the effective stress of the overlying strata, and the compaction is strong. The organic matter pores are affected to deform, narrow or even close. Semi-closed-semi-open system has good sealing property during hydrocarbon generation period at the edge and outside the rift trough, which is conducive to the in-situ retention of hydrocarbons and the formation and preservation of pores. In the later stage, the strength of structural transformation is weak, and a better gas-rich interval is formed.

5.1.3. *Effect of overpressure of hydrocarbon fluid on pore preservation*

The overpressure of reservoir fluid can resist pressure and preserve pores. With the cracking of kerogen and retained hydrocarbons to form gaseous hydrocarbons, the pore fluid pressure increases continuously. Under good storage conditions, the pore system retained a large amount of gaseous hydrocarbons is in an overpressure state, which can offset the effect of overlying pressure and tectonic stress, and play a constructive role in maintaining organic pores under deep burial conditions. The pore volume and pore specific surface area inside and outside the rift trough show a decreasing trend (Table 1), the Feret diameter of the pores gradually becomes larger and the roundness gradually becomes smaller (Fig. 6). The macropores in the rift trough are well preserved and contribute greatly to the reservoir space. The edge of the rift trough gradually becomes smaller, but it still has a certain contribution, the contribution of mesopores increases. The contribution of macropores outside the rift trough further decreases, and the contribution of micropores and mesopores increases (Fig. 7(d) and (e)). The 5th layer of Qiongzhusi Formation has appropriate quartz content, a small amount of clay content and the most feldspar content (Fig. 2). On the basis of the development of organic pores, the inorganic matter is relatively more developed. The pressure coefficient of Q3 well in the rift trough is 2.01, and the system is a closed system. The hydrocarbon expulsion during the maximum hydrocarbon generation period is weak, and

Table 1
Basic elements and production statistics of typical well gas reservoirs inside and outside the rift trough.

Geologic accumulation element	Q1	Q2	Q3
Depositional environment	Shallow shelf	Semi-deep–deep shelf	Deep shelf
Depth, m	3000–3300	4000–4500	4000–5000
Pressure coefficient	1.01	1.73	2.01
Porosity, %	3.54	3.67	4.60
Pore volume, g/cm^3	0.014	0.018	0.021
Pore specific surface area, m^2/g	10.46	10.80	16.93
Testing production, 10^4 m^3/d	0.20	38.60	73.88

the hydrocarbon fluid in the pores maintains overpressure (Fig. 10(c)), the pores are best preserved, and the porosity is higher. Due to the absence or erosion of the floor (Maidiping Formation) outside the rift trough, the Qiongzhusi Formation is directly in contact with the dolomite of the Dengying Formation. The organic-rich shale in the bottom of Qiong1^{1}member generates a large amount of hydrocarbon, forming overpressure, but the system is an open system. It begins to discharge a large number of hydrocarbons along the unconformity surface, and the hydrocarbons migrate downward. Subsequently, the Himalayan paleo-uplift was reactivated, and the Weiyuan area outside the trough was lifted by a large margin (Fig. 10(a)). The pre-existing cracks at

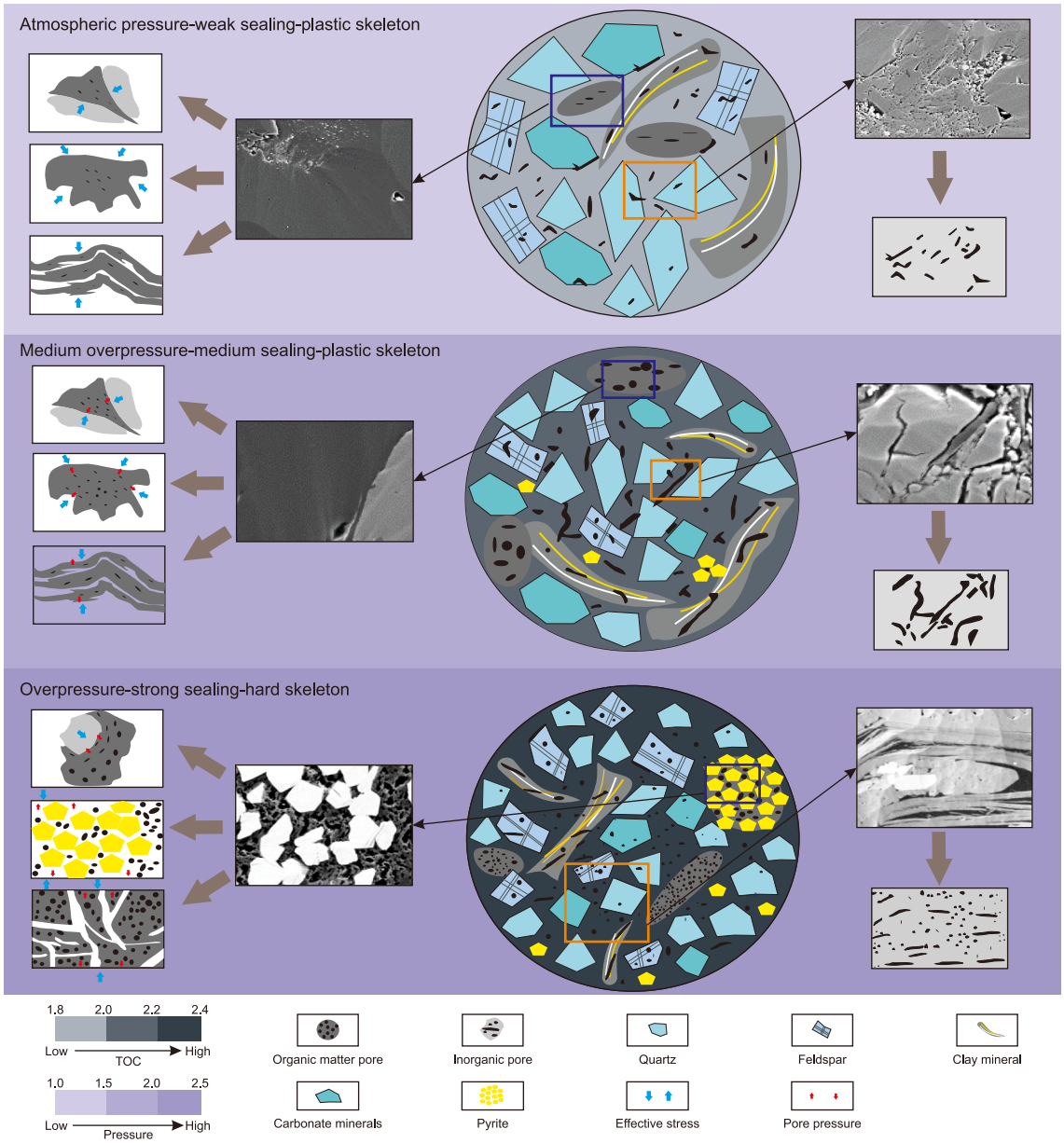

Fig. 13. Conceptual model of shale pore preservation mechanism of Qiongzhusi Formation inside and outside the rift trough.

the bottom of the 1st layer opened, the gas was lost along the interlayer slip joints, and the pressure system outside the trough was further destroyed (Q1 well pressure coefficient 1.01), resulting in further compaction and destruction of the pores. The pores are in contact with the surface-sewn line, and the pore closure degree is high. According to the actual production data, the Q3 well testing production is 73.88 $\times$ 10^4 m^3/d. The Q2 well testing production is 38.6 $\times$ 10^4 m^3/d. The Q1 well testing production is 0.2 $\times$ 10^4 m^3/d (Table 1).

5.2. Conceptual model of pore preservation in fine-grained sedimentary rocks

The deep-water shelf facies deposits (Fig. 1(a)) and fine-grained deposits (Figs. 3 and 4(b)) are found in the rift trough. The mineral composition is dominated by quartz and feldspar minerals, with a small amount of clay minerals and high organic matter content (Fig. 2). The reservoir space is mainly composed of organic matter pores, intergranular pores and dissolution pores of feldspar and clay minerals. The shape is elliptical and slit-like (Fig. 5(g)–(i)), with high pore specific surface area and pore volume. Meso–macro pores contribute greatly to reservoir space. Quartz has authigenic quartz, which can form a rigid character frame (Fig. 11(b), (e) and (f)). The uplift amplitude is weak, and the system is closed during the maximum hydrocarbon generation period, a small amount of hydrocarbon is expelled, a large number of retained hydrocarbons are cracked, and the hydrocarbon fluid in the pores is overpressured (Figs. 10(c) and 12). The pores are protected by rigid framework, system closure and hydrocarbon fluid overpressure, so that after the uplift of gas reservoir, the pores are still open and have high porosity characteristics, which further leads to high yield (Table 1). The pore preservation mode in the rift trough is overpressure-strong sealing-hard skeleton type (Fig. 13).

The margin of the rift trough is a semi-deep–deep-water shelf facies deposit. The sedimentary grain size becomes coarser (Figs. 3 and 4(c)), the content of feldspar decreases, the content of clay minerals increases, and the content of organic matter decreases (Fig. 2). The reservoir space is mainly composed of clay mineral intergranular pores, feldspar mineral dissolution pores and cracks, and a small amount of organic matter pores. The shape is mainly long and wedge-shaped (Fig. 5(d)–(f)). The pore specific surface area and pore volume are slightly reduced, the mesopores contribute the most to the reservoir space, and the macropores contribute less (Fig. 7). Quartz is dominated by terrigenous quartz and lacks rigid framework support (Fig. 11(a) and (c)). After the maximum burial depth, the uplift range is moderate. The system is relatively closed during the maximum hydrocarbon generation period, with moderate hydrocarbon expulsion and retention of hydrocarbon cracking. The fluid in the pores maintains moderate overpressure (Figs. 10(b) and 12). The pores are mainly protected by compartment system and medium overpressure of the fluid. Under the condition of small burial depth, most of the pores remain open, and a small amount is closed due to the influence of overlying strata stress. The porosity is slightly lower than that in the rift trough, and the yield is moderate (Table 1). The margin of rift trough is medium overpressure-medium closure-plastic skeleton pore preservation mode (Fig. 13).

Outside the rift trough is the shallow shelf facies with the coarsest grain size (Figs. 3 and 4(c)). The content of clay minerals decreases and carbonate minerals increases (Fig. 2). The reservoir space is composed of inorganic mineral intergranular pores and a small amount of dissolution pores, and organic matter pores are not developed. The morphology is dominated by long strips and wedges (Fig. 5(a)–(c)). The pore specific surface area and pore volume are further reduced, the contribution of mesopores and macropores to reservoir space is reduced, and the contribution of micropores is increased (Fig. 7). Quartz is dominated by terrigenous quartz and lacks rigid framework support (Fig. 11). After the maximum burial depth, the uplift range is large, the system is relatively open during the maximum hydrocarbon generation period, a large amount of hydrocarbon is expelled, a small amount of retained hydrocarbon is cracked, and the fluid in the pores is normal pressure (Figs. 10(a) and 12(c)). The pores are not effectively protected. Under the condition of small burial depth outside the trough, most of the pores have been closed, the porosity is further reduced, and the production is the smallest (Table 1). The pore preservation mode outside the rift trough is normal pressure–weak closure–plastic skeleton type (Fig. 13).

6. Conclusions

The preservation of pores is governed by mineral composition and the presence of a rigid skeletal framework. Within the rift trough, a rigid mineral skeleton composed of authigenic quartz and pyrite effectively resists compaction, thereby preserving the integrity of both organic pores (round to oval) and inorganic pores (dissolution and intergranular types). In contrast, outside the trough, a plastic skeleton dominated by terrigenous clastic minerals leads to pronounced pore closure, resulting in a porosity (3.54%) of 34% lower than that inside the trough (4.60%).

Pore evolution is further controlled by the sealing capacity of the compartment system and the presence of overpressure. The closed system and associated hydrocarbon overpressure in the rift trough inhibit pore compaction by counteracting overlying stress. Outside the trough, however, an open system leads to the dissipation of overpressure, accompanied by a 90% reduction in porosity with increasing burial depth.

A ternary coupling pore preservation model of pore preservation “rigid skeleton–compartment system–hydrocarbon fluid overpressure” was established for Qiongzhusi Formation shale. This model highlights the combined roles of tectonic-sedimentary differentiation, mineral composition governed by sedimentation, and system sealing and fluid overpressure influenced by structure. The rift trough exhibits an overpressure–strong sealing–rigid skeleton pore preservation mode, which supports high gas yield. In contrast, outside the trough, a normal pressure–weakly closed–plastic skeleton mode dominates, where gas production is only 0.3% of inside rift trough.

CRediT authorship contribution statement

Dan-Dan Wang: Writing – review & editing, Writing – original draft. **Zhen-Xue Jiang:** Funding acquisition, Conceptualization. **Ma-Jia Zheng:** Software, Resources. **Ya Wu:** Methodology, Investigation. **Huan Miao:** Software, Investigation. **Zhi-Kai Liang:** Data curation. **Yun-Hao Zhang:** Formal analysis. **Da-Dong Liu:** Investigation. **Xiang-Lu Tang:** Formal analysis.

Data availability

Data not included in the figures and tables of the manuscript can be requested from the corresponding author.

Declaration of competing interest

The authors declare that they have no known competing financial interests or personal relationships that could have appeared to influence the work reported in this paper.

Acknowledgments

This study was funded by Innovative Research Group Project of the National Natural Science Foundation of China (grant Nos. U24A20592 and 42272137) and Guizhou Province Science and Technology Innovation Talent Team: Construction of the Science and Technology Innovation Talent Team for the Evaluation and Development of Unconventional Natural Gas Resources in Complex Structural Areas (No. Qian Ke He Platform Talent-CXTD[2023]013).

References

Aplin, A.C., Macquaker, J.H.S., 2011. Mudstone diversity: origin and implications for source, seal, and reservoir properties in petroleum systems. AAPG Bull. 95 (12), 2031–2059. https://doi.org/10.1306/03281110162.

Duan, Z.H., Moller, N., Weare, J.H., 1992. An equation of state for theCH_4-CO_2-H_2O system: I. Pure systems from 0 to 1 000 °C and 0 to 8000 bar. Geochem. Cosmochim. Acta 56 (7), 2605–2617. https://doi.org/10.1016/0016-7037(92)90347-L.

Fan, H.J., Deng, H.C., Fu, S.Y., et al., 2021. Sedimentary characteristics of the Lower Cambrian qiongzhusi Formation in the Sichuan Basin and its response to construction. Acta Sedimentol. Sin. 39 (4), 1004–1019. https://doi.org/10.14027/j.issn.1000-0550.2020.041 (in Chinese).

Gao, J., He, S., He, Z.L., et al., 2014. Genesis of calcite vein and its implication to petroleum preservation in Jingshan region, Mid-Yangtze. Oil Gas Geol. 35 (1), 33–41. https://doi.org/10.11743/ogg20140105 (in Chinese).

Guan, Q.Z., Dong, D.Z., Zhang, H.L., et al., 2021. Types of biogenic quartz and its coupling storage mechanism in organic-rich shales: A case study of the Upper Ordovician Wufeng Formation to Lower Silurian Longmaxi Formation in the Sichuan Basin, SW China. Petrol. Explor. Dev. 48 (4), 700–709. https://doi.org/10.1016/S1876-3804(21)60068-X (in Chinese).

Guo, Q.L., Mi, J.K., Wang, J., et al., 2019. An improved hydrocarbon generation model of source rocks and key parameter templates. China Petrol. Expl. 24 (5), 661–669. https://doi.org/10.3969/j.issn.1672-7703.2019.05012 (in Chinese).

Guo, Q.Y., Xu, S., Hao, F., et al., 2021. The effect of tectonic deformation and preservation condition on the shale pore structure using adsorption-based textural quantification and 3D image observation. Energy 219, 119579. https://doi.org/10.1016/j.energy.2020.119579.

Guo, X.S., Hu, D.F., Yu, L.J., et al., 2023. Study on the micro mechanism of shale self-sealing and shale gas preservation. Petrol. Geol. Exp. 45 (5), 821–831. https://doi.org/10.11698/PED.2021.03.01 (in Chinese).

Guo, T.L., Xiong, L., Ye, S.J., et al., 2023b. Theory and practice of unconventional gas exploration in carrier beds: insight from the breakthrough of new type of shale gas and tight gas in Sichuan Basin, SW China. Petrol. Explor. Dev. 50 (1), 24–37. https://doi.org/10.1016/S1876-3804(22)60367-7.

Guo, T.L., Xiong, L., He, J.H., et al., 2024. New type shale gas exploration discovery and enlightenment of the Lower Cambrian qiongzhusi Formation in the Southern Sichuan Basin. J. Southwest Petrol. Unive. (Sci. Tech. Ed.) 46 (6), 1–14. https://doi.org/10.11885/j.issn.1674.5086.2024.11.20.29 (in Chinese).

He, L.J., Xu, H.H., Wang, J.Y., 2011. Hermal evolution and dynamic mechanism of the Sichuan Basin during the early permian-Middle Triassic. Sci. China Earth Sci. 54 (12), 1948–1954. https://doi.org/10.1007/s11430-011-4240-z.

Jia, C.Z., Pang, X.Q., Song, Y., 2021. The mechanism of unconventional hydrocarbon formation: hydrocarbon self-containment and intermolecular forces. Petrol. Explor. Dev. 48 (3), 437–452. https://doi.org/10.11698/PED.2021.03.01 (in Chinese).

Lazar, O.R., Bohacs, K.M., Macquaker, J.H.S., et al., 2015. Capturing key attributes of fine-grained sedimentary rocks in outcrops, cores, and thin sections: nomenclature and description guidelines. J. Sediment. Res. 85, 230–246. https://doi.org/10.2110/jsr.2015.11.

Li, C.R., 2021. Hydrocarbon Generation and Expulsion History Reconstruction and Hydrocarbon Resource Potential Evaluation of Lower Cambrian post-to Over-mature Source Rocks in the Sichuan Basin. Doctoral Dissertation. China University of Petroleum (Beijing), Beijing (in Chinese).

Li, W., He, S., Zhang, B., et al., 2018. Palaeotemperature and palaeopressure characteristics of fluid inclusions in shale composite veins of the Longmaxi Formation in the western margin of Jiaoshiba anticline. Acta Pet. Sin. 39 (4), 402–415. https://doi.org/10.7623/syxb201804004 (in Chinese).

Li, X.Y., Chen, S.B., Wu, J.F., et al., 2024. Dynamic variation of full-scale pore compressibility and heterogeneity in deep shale gas reservoirs: Implications for pore system preservation. Energy Fuels 38, 3880–3899. https://doi.org/10.1021/acs.energyfuels.3c04097.

Liang, X., Shan, C.A., Zhang, C., et al., 2021. "Three dimensional closed system" accumulation model of Taiyang anticline mountain shallow shale gas in the Zhaotong demonstration area. Acta Geol. Sin. 95 (11), 3380–3399. https://doi.org/10.19762/j.cnki.dizhixuebao.2021145 (in Chinese).

Liang, Z.K., Jiang, Z.X., Xue, Z.X., et al., 2024. Experimental investigation of kerogen structure and heterogeneity during pyrolysis. Geoenergy Sci. Eng. 242, 213222. https://doi.org/10.1016/j.geoen.2024.213222.

Liu, R.Y., 2023. Shale Gas Reservoir Characteristics and Enrichment Patterns of the Qiongzhusi Formation in the Weiyuan Area of the Sichuan Basin. Doctoral Dissertation. Chengdu University of Technology, Chengdu (in Chinese).

Liu, W.X., Lu, L.F., Ye, D.L., et al., 2022. Significance and formation mechanism of abnormally pressured compartments of shale gas in the Ordovician Wufeng-Silurian Longmaxi formations, southeastern Sichuan Basin. Petrol. Geol. Exp. 44 (5), 804–814. https://doi.org/10.11781/sysydz202205804 (in Chinese).

Mei, Q.H., He, D.F., Wen, Z., et al., 2014. Geologic structure and tectonic evolution of Leshan-Longnvsi paleo-upliftin Sichuan Basin, China. Acta Pet. Sin. 35 (1), 11–25. https://doi.org/10.7623/syxb201401002 (in Chinese).

Milliken, K.L., 2014. A compositional classification for grain assemblages in fine-grained sediments and sedimentary rocks. J. Sediment. Res. 84 (12), 1185–1199. https://doi.org/10.2110/jsr.2016.2.

Milliken, K.L., Curtis, M.E., 2016. Imaging pores in sedimentary rocks: foundation of porosity prediction. Mar. Petrol. Geol. 73, 590–608. https://doi.org/10.1016/j.marpetgeo.2016.03.020.

Nie, H.K., Liu, Q.Y., Li, P., et al., 2025. Quartz types, formation mechanism, and its effect on shale oil and gas enrichment: A review. Earth Sci. Rev. 261, 105011. https://doi.org/10.1016/j.earscirev.2024.105011.

Qiu, N.S., Liu, W., Fu, X.D., et al., 2021. Maturity evolution of Lower Cambrian Qiongzhusi Formation shale of the Sichuan Basin. Mar. Petrol. Geol. 128, 105061. https://doi.org/10.1016/j.marpetgeo.2021.105061.

Rao, S., Zhu, C.Q., Tang, X.Y., et al., 2013. Thermal evolution patterns of the Sinian-Lower Paleozoic source rocks in the Sichuan Basin, southwest China. Chin. J. Geophys. 56 (5), 1549–1559. https://doi.org/10.6038/cjg20130513 (in Chinese).

Rao, S., Yang, Y.N., Hu, S.B., et al., 2022. Thermal evolution history and shale gas accumulation significance of Lower Cambrian qiongzhusi Formation in Southwest Sichuan Basin. Earth Sci. 47 (11), 4319–4335. https://doi.org/10.3799/dqkx.2022.153 (in Chinese).

Richardson, N.J., Densmore, A.L., Seward, D., et al., 2008. Extraordinary denudation in the Sichuan Basin: Insights from low-temperature thermochronology adjacent to the eastern margin of the Tibetan Plateau. J. Geophys. Res. 113 (B044094), 1–23. https://doi.org/10.1029/2006JB004739.

Shi, Y.Z., Wang, Z.C., Xu, Q.C., et al., 2024. Reconstruction and application of thermal history of old strata in superimposed basin: A case study on the Sinian-Cambrian in the central Sichuan paleo-uplift of the Sichuan Basin. Nat. Gas. Ind. 44 (8), 29–43. https://doi.org/10.3787/j.issn.1000-0976.2024.08.003 (in Chinese).

Su, G.P., 2021. Study on structural characteristics and tectonic evolution in the northern slope of central Sichuan Paleo-uplift and their influences on Hydrocarbon accumulation. Doctoral Dissertation. Chengdu university of technology, Chengdu (in Chinese).

Wang, Y.M., Dong, D.Z., Yang, H., et al., 2014. Quantitative characterization of reservoir space in the Lower Silurian Longmaxi Shale, southern Sichuan, China. Sci. China Earth Sci. 44 (6), 1348–1356. https://doi.org/10.1007/s11430-013-4645-y (in Chinese).

Wang, R.Y., Nie, H.K., Hu, Z.Q., et al., 2020. Controlling effect of pressure evolution on shale gas reservoirs: A case study of the Wufeng–Longmaxi formations in the Sichuan Basin. Nat. Gas. Ind. 40 (10), 1–11. https://doi.org/10.3787/j.issn.1000-0976.2020.10.001 (in Chinese).

Wang, D.D., Jiang, Z.X., Yang, Y., Shao, X.D., Feng, X., Du, W., Shi, F.L., Chen, W.Y., 2023. Under the control of multi-stage structure shallow, normal-pressure shale gas accumulation characteristics in Fuyan syncline of northern Guizhou. Energy Fuels 37 (21), 16599–16611. https://doi.org/10.1021/acs.energyfuels.3c03339.

Wang, D.D., Jiang, Z.X., Du, W., et al., 2025. Pore structure difference characteristics and evolution model in the process of gas reservoir uplift: A case study of the shale reservoir of Wufeng Formation-Longmaxi Formation in Sichuan Basin and its surrounding areas. Acta Geol. Sin. 99 (4), 1381–1397. https://doi.org/10.19762/j.cnki.sizhixuebao.2024090 (in Chinese).

Xiang, M., Xu, S., Wen, Y.R., et al., 2024. 2024. Influence of tectonic preservation conditions on the nanopore structure of shale reservoir: A case study of Wufeng-Longmaxi formations shale in western Hubei area, south China. Pet. Sci. 21, 2203–2217. https://doi.org/10.1016/j.petsci.2024.02.008.

Xiong, L., Deng, H.C., Wu, D., et al., 2023. Fine-grained sedimentary characteristics and influencing factors of the Lower Cambrian Qiongzhusi Formation in Sichuan Basin and on its periphery. Petrol. Geol. Exp. 45 (5), 857–871. https://doi.org/10.11781/sysydz202305857 (in Chinese).

Xu, H.L., Wei, G.Q., Jia, C.Z., et al., 2012. Tectonic evolution of the Leshan-Longnüsi paleo-uplift and its control on gas accumulation in the Sinian strata, Sichuan Basin. Petrol. Explor. Dev. 39 (4), 406–416. https://doi.org/10.1016/S1876-3804(12)60060-3 (in Chinese).

Yong, R., Wu, J.f., Wu, W., et al., 2024. Exploration discovery of shale gas in the Cambrian Qiongzhusi Formation of Sichuan Basin and its significance. Acta

Pet. Sin. 45 (9), 1309–1323. https://doi.org/10.11698/PED.20230616 (in Chinese).
Yu, W.M., Yuan, S.S., Tang, H.X., et al., 2024. The effect of structural preservation conditions on pore structure of marine shale reservoir: A case study of the Wufeng-Longmaxi Formation shale, Southern Sichuan Basin, China. Front. Earth Sci. 12, 1360202. https://doi.org/10.3389/feart.2024.1360202.
Zhang, M.M., Li, Z., 2018. The lithofacies and reservoir characteristics of the fine-grained sedimentary rocks of the Permian Lucaogou Formation at the northern foot of Bogda Mountains, Junggar Basin (NW China). J. Petrol. Sci. Eng. 170, 21–39. https://doi.org/10.1016/j.petrol.2018.06.007.
Zhang, K., Song, Y., Jia, C.Z., et al., 2022. 2022. Formation mechanism of the sealing capacity of the roof and floor strata of marine organic-rich shale and shale itself, and its influence on the characteristics of shale gas and organic matter pore development. Mar. Petrol. Geol. 140, 105647. https://doi.org/10.1016/j.marpetgeo.2022.105647.
Zhao, J.H., Jin, Z.J., Lin, C.S., et al., 2019. Sedimentary environment of the Lower Cambrian Qiongzhusi Formation shale in the Upper Yangtze region. Oil Gas Geol. 40 (4), 701–715. https://doi.org/10.11743/ogg20190402 (in Chinese).
Zhu, B.Y., 2024. Study on multi-scale Characteristics and Methods of Organic Matter Pore Space in Deep Marine Shale. Doctoral Dissertation. Yangtze university, Wuhan (in Chinese).